Nonlinear Dyn
DOI 10.1007/s11071-007-9329-8

ORIGINAL PAPER

Hysteresis models of dynamic mode atomic force microscopes: analysis and identification via harmonic balance

Michele Basso · Donatello Materassi · Murti Salapaka

Received: 1 August 2007 / Accepted: 26 December 2007

Abstract A new class of models based on hysteresis functions is developed to describe the operation of dynamic mode atomic force microscopy. Such models can account for dissipative phenomena affecting the interaction between the probe and the sample. The model analysis, which is developed using frequency domain techniques, provides a insights into experimentally observed behavior. Experimental data corroborates the models developed.

Keywords Atomic force microscopy · Hysteresis · Harmonic balance · Identification · Nanotechnology · Lur'e system

1 Introduction

Physical systems with impact phenomena are frequent in many fields [1]. Main applications occur in mechanics where macroscopic objects are considered. In the macroscopic case, an impulsive approximation for interaction forces with a pure repulsive nature can often be correctly assumed. Moreover, energy losses are traditionally considered by introducing the concept of coefficient of restitution [2, 3]. However, there are many situations when this kind of approximation cannot be considered satisfactory, for example, when the interaction involves both attractive and repulsive forces or when the interaction cannot be assumed instantaneous. The aim of this work is to exploit a hysteresis function to model the related interaction forces. This new model can be viewed as a generalization of the impulsive case and allows for the use of potential functions even if the system is dissipative. It also presents advantages when the interaction involves both repulsive and attractive parts or when the duration of the impact is not negligible. In addition, the hysteresis model facilitates the use of powerful analysis techniques, such as harmonic balance [4], which cannot be used for impulsive forces. To show how the impact model can be successfully employed, its application to an Atomic Force Microscope (AFM) is demonstrated. Specifically, we limit ourselves to the study of an AFM operating in dynamic mode, with the schematic depicted in Fig. 1 that shows a cantilever that is periodically forced by a piezo placed under its support inducing a periodic oscillation. The cantilever dynamics are also influenced by interaction forces between the cantilever tip and the sample. The topography can be inferred by slowly moving the cantilever laterally along the sample surface

M. Basso · D. Materassi (✉)
Dipartimento di Sistemi e Informatica, Università di Firenze, via S. Marta, 3, 50139 Firenze, Italy
e-mail: materassi@dsi.unifi.it

M. Basso
e-mail: basso@dsi.unifi.it

M. Salapaka
Electrical and Computer Engineering Department, University of Minnesota, Minneapolis, MN 55455, USA
e-mail: murti@umn.edu

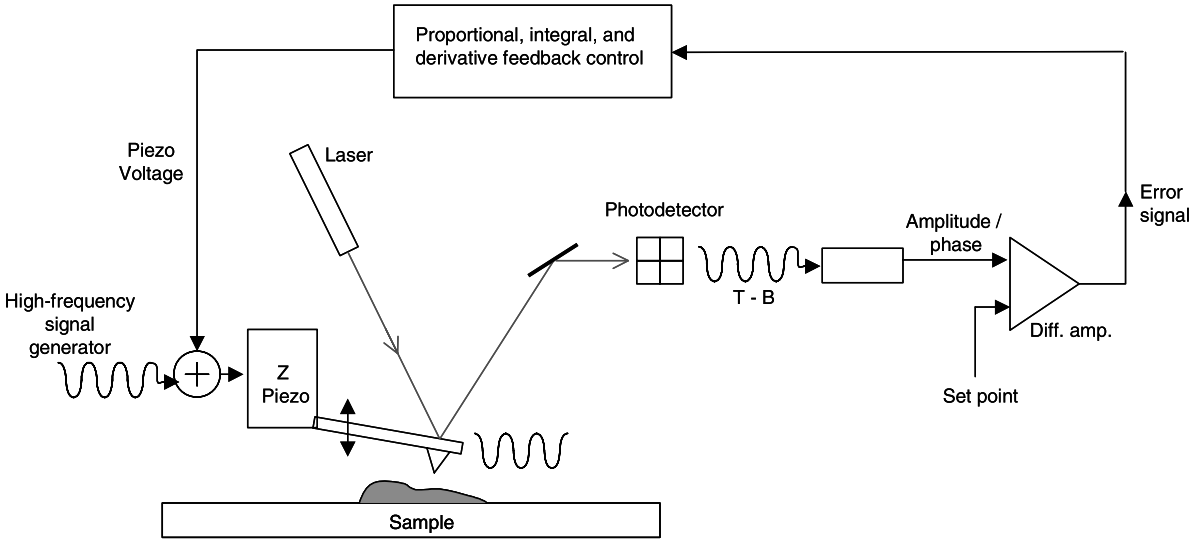

Fig. 1 Schematic of a dynamic-mode AFM

by means of a positioning system and by measuring the amplitude of the first harmonic (of the forcing frequency) of the cantilever oscillation. The deflection of the cantilever is measured through an optical lever method. A feedback controller driving the input voltage to the z piezo is employed to reject variations of the separation between the sample and the tip due to the sample topography. Apart from the topography of the sample, another primary use of AFM is the study of force interactions. Two methods are prevalent. The cantilever-sample offset (also termed as separation), which is the distance between the cantilever holder and the z piezo positioner is first reduced by the piezo positioner, where the sample surfaces approaches the cantilever-tip. In the retract phase, the cantilever-sample offset is increased by using the piezo positioner. During the approach and the retract phases, the cantilever deflection signal is recorded. The force felt by the cantilever can be obtained by multiplying the deflection by its spring-constant. By plotting the force felt by the cantilever against the cantilever-sample offset, the force curves are obtained. These curves are called static force curves. In dynamic force curves, the cantilever is oscillated using the dither piezo. The amplitude of the first harmonic is plotted against the cantilever-sample offset during the approach and retract phases. The dynamic force curves are gentler on the sample, and therefore, are the preferred means of investigating samples that are soft (for example, biological matter). A difficulty of using the dynamic mode when compared to static mode in obtaining force curves is that determining force-separation curves from the measured amplitude-separation curves is not straightforward. In most cases, dynamic force curves are obtained by intensive numerical simulation. For example, in [5] and [6], models that accurately describe the device behavior are proposed. In another approach, parametrized models of the tip sample interaction are assumed, the parameters identified using the amplitude-separation data, and subsequently, the force-curve data is generated using the identified model. In [7] an identification algorithm of the force-curve is obtained by the numerical computation of an explicit integral equation. Analytical results can be found in [8], where a simple impulsive impact model is developed. However, since the employed model neglects attractive forces, it cannot explain important characteristics of the tip-sample interaction observed in experiments. Similarly, in [9], an analytical equation for amplitudes and forces (average values) is derived based on the virial theorem and energy conservation principles.

In this work, we develop a frequency-based analysis method of a dynamic-mode AFM. We propose hysteresis models that take into account attractive forces in the sample-cantilever interaction. The main feature of the proposed model is to provide results without the

means of numerical simulations, for example, evaluating the amplitude-separation curve for a large class of interaction forces comprising of the common potential functions studied in the literature, such as the classical Lennard–Jones potential [10]. Other attractive features of the proposed class of models are: (i) it can account for energy losses; (ii) it is suited for nonlinear frequency-domain identification techniques such as those proposed in [6] and [11]; and (iii) it facilitates the study of structural properties of the system such as bifurcation phenomena experimentally observed exploiting frequency domain techniques as in [12]. Identification results based on experimental data are provided where the hysteresis model gives a good qualitative and quantitative characterization of the tip-sample behavior.

The paper is organized as follows. In Sect. 2, we briefly describe the general problem of modeling an impact. In Sect. 3, we exploit such a model to describe the AFM dynamic-mode behavior and in Sect. 4, a frequency analysis is provided using harmonic balance techniques. In Sect. 5, the identification procedure is described, and finally in Sect. 6, experimental results are discussed.

2 Hysteresis functions to model a collision

Let P_1 and P_2 be two material objects with masses m_1 and m_2, respectively, moving along the x axis, with position x_1 and x_2 ($x_1 < x_2$). We consider P_1 and P_2 subject to external forces $f_1(t)$ and $f_2(t)$, respectively, and to a mutual internal force. P_1 exerts a force on P_2 given by h_2 and P_2 exerts an equal and opposite force h_1 on P_1. The interaction force h_i are dependent on time t, relative separation $x_1 - x_2$ and relative velocity $\dot{x}_1 - \dot{x}_2$. The following dynamical relations describe the system

$$\begin{cases} m_1\ddot{x}_1 = f_1(t) + h_1(t, x_2 - x_1, \dot{x}_2 - \dot{x}_1), \\ m_2\ddot{x}_2 = f_2(t) + h_2(t, x_2 - x_1, \dot{x}_2 - \dot{x}_1). \end{cases} \tag{1}$$

Earlier interaction models usually neglected dissipation losses or used a constant coefficient of restitution to account for such losses. Defining $\delta := x_2 - x_1$, we suppose that the interaction between the two masses is negligible outside a time interval $[t_s, t_f]$ where $\delta(t_s) = \delta(t_f)$. We assume that the system dynamics can be split in two different phases: an "approach phase" in the time interval $[t_s, \bar{t}]$ where $\dot{\delta} \leq 0$ and a "retract phase" in the time interval $[\bar{t}, t_f]$ where $\dot{\delta} \geq 0$. We also consider that $\delta(t)$ is a continuous function and that the set of points where $\dot{\delta} = 0$ has zero measure. The model we will employ in this work defines a particular form for the interaction forces, and at the same time, allows one to generalize the case of constant coefficient of restitution that is not restricted to the cases with instantaneous impact time. In addition, it presents advantages in the study of periodic systems with impact behavior. The interaction force assumes the following two different forms during the approach and the retract phases

$$h(\delta, \dot{\delta}) := \begin{cases} h^+(\delta) & \text{if } \dot{\delta} > 0, \\ h^-(\delta) & \text{if } \dot{\delta} < 0. \end{cases} \tag{2}$$

The simplicity of the dependence of h on the sign of $\dot{\delta}$ leads to a tractable analysis while capturing the prominent features of finite nonzero interaction time that can have both attractive as well as repulsive forces.

If h^+ and h^- are integrable, then the potential functions U^+ and U^- can be introduced with

$$\begin{aligned} U^+(\delta) &= -\int_{\delta(t_s)}^{\delta} h^+(x)\,\mathrm{d}x \\ U^-(\delta) &= -\int_{\delta(t_s)}^{\delta} h^-(x)\,\mathrm{d}x. \end{aligned} \tag{3}$$

As $h^-(\delta) > h^+(\delta)$, for all $\delta < \delta(t_s)$, we have that $U^-(\delta) > U^+(\delta)$ for all $\delta < \delta(t_s)$. Considering the instant $\bar{t}$ when the relative distance $\delta(t)$ is the smallest, we can state that the potential interaction energy is $U^-(t)$ if $t < \bar{t}$, while it is $U^+(t)$ if $t > \bar{t}$. At any instant, the interaction force is conservative except at $t = \bar{t}$ when the relative velocity is zero and we have an "instantaneous" energy variation ΔE equal to

$$\Delta E = U^-\big(\delta(\bar{t})\big) - U^+\big(\delta(\bar{t})\big). \tag{4}$$

The energy lost in the impact can be interpreted as the area between the curves $h^-(\delta)$ and $h^+(\delta)$ in the interval $[\delta(\bar{t}), \delta(t_s)]$. In the next section, we will show how this class of hysteresis functions can be exploited to analyze and identify tip-sample interactions in AFMs.

3 AFM model

AFM cantilevers can be modeled as a feedback interconnection of a linear system $\mathcal{L}$ and a nonlinear static function h as depicted in Fig. 2. Models with this structure are well known as Lur'e models [4]. The system equation can be written using the symbolic form as

$$y(t) = L\left(\frac{\mathrm{d}}{\mathrm{d}t}\right)\left[h\big(\delta(t), \dot{\delta}(t)\big) + \gamma(t)\right] \tag{5}$$

where $y(t)$ is the measured output (that is the cantilever tip deflection), l, apart an additive constant, is the separation, $\delta(t) = y(t) + l$ is the tip-sample distance, and $\gamma(t)$ is the external periodic forcing

$$\gamma(t) = \Gamma \cos(\omega t + \phi).$$

The subsystem $\mathcal{L}$ describes the free cantilever dynamics, whose frequency response $L(i\omega)$ can be precisely identified using thermal noise or a simple frequency sweep excitation when the sample is absent [13].

The feedback subsystem h accounts for the sample interaction force, which is a nonlinear function of the tip-sample distance δ. The main difficulty in modeling h lies in the choice of a suitable class of functions to describe the force potential. It is a common choice to consider h as the sum of a conservative force h_{con} and a dissipative force h_{dis}, that is,

$$h(\delta, \dot{\delta}) = h_{\mathrm{con}}(\delta) + h_{\mathrm{dis}}(\delta, \dot{\delta}), \tag{6}$$

h_{dis} is typically given a simple form to allow easy computation [14]. Also in [14], it is proposed that

$$h_{\mathrm{dis}}(\delta, \dot{\delta}) = \Gamma(\delta)\dot{\delta} \tag{7}$$

where Γ represents a damping coefficient.

In this paper, we consider the following class of hysteresis functions which generalizes the one presented in [15]

$$h(\delta, \dot{\delta}) = \begin{cases} \sum_{n=1}^{N} K_n^- h_n(\delta) & \text{if } \dot{\delta} < 0, \\ \sum_{n=1}^{N} K_n^+ h_n(\delta) & \text{if } \dot{\delta} \geq 0 \end{cases} \tag{8}$$

where $h_n(\delta)$ are nonnegative functions where the dependence of h on $\dot{\delta}$ is only on its sign. The interaction described by $h(\delta, \dot{\delta})$ can include dissipative terms by adding constraints on the parameters K_n^+ and K_n^-. For example, the condition

$$K_n^- \geq K_n^+ \tag{9}$$

makes the contribution of every element h_n dissipative over the interval $[t_s\ t_f]$.

In our analysis, we will consider two special cases of this hysteretic interaction. This way of modeling dissipations has already been proposed in [16] and has been successfully exploited by [15] in an identification procedure.

3.1 Piecewise interaction force

The first class of potential functions we treat contains the functions $h(\cdot)$ in the form (8) where $N = 2$ and

$$h_n(\delta) = \begin{cases} 0 & \text{if } \delta \geq 0, \\ |\delta|^{n-1} & \text{if } \delta < 0. \end{cases} \tag{10}$$

In Fig. 3, such a kind of function is depicted. Since $\delta = y + l$, here the parameter l models the offset at which the tip-sample interaction forces become effective.

3.2 Lennard–Jones-like interaction force

The Lennard–Jones potential

$$h(\delta) = \frac{K_{n_a}}{\delta^{n_a}} + \frac{K_{n_r}}{\delta^{n_r}}, \quad n_a < n_r \in \mathcal{N};\ K_{n_a}, K_{n_r} \in \mathcal{R} \tag{11}$$

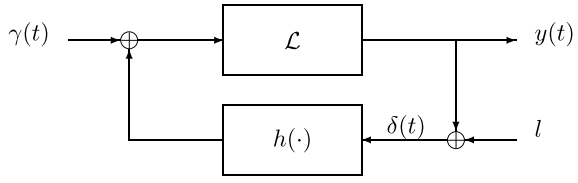

Fig. 2 A feedback interconnection of a linear system and a nonlinear static function

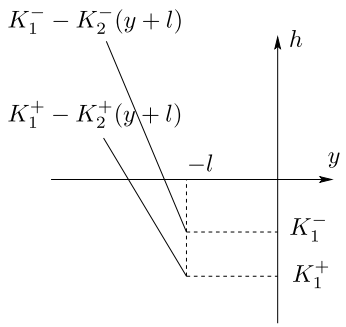

Fig. 3 Interaction force modeled by a piecewise linear function

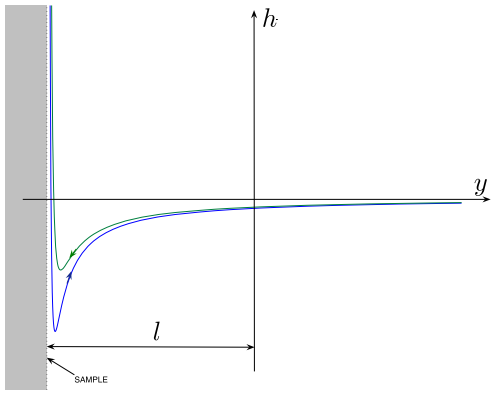

Fig. 4 Sketch of a Lennard–Jones-like interaction with hysteresis

is a common choice of modeling the potential between atoms (see [17]). We consider a generalization of the Lennard–Jones potential in the form (8) where

$$h_n(y) = \frac{1}{\delta^n}. \tag{12}$$

The parameter l represents the offset where the interaction force becomes infinitely large (Fig. 4). The choice of this class of functions is motivated by its simplicity, and also by the fact that long-range dissipative interfacial forces have already been successfully modeled using a time-dependent power law where the strength of the force depends only on whether the probe approaches or retracts away from the sample [15].

4 Frequency analysis via harmonic balance

The linear part of the Lur'e system given by $\mathcal{L}$ in (5) typically shows a sharp filtering effect beyond the first resonance peak because of a high quality factor of the cantilever. Indeed, it is experimentally observed that the cantilever trajectory has a quasi-sinusoidal behavior. The cantilever-tip motion can be approximated by

$$\begin{aligned} y(t) \simeq y_1(t) &:= \mathrm{Re}\big[A + B\mathrm{e}^{i\omega t}\big] \\ &= A + B\cos(\omega t). \end{aligned} \tag{13}$$

The corresponding output of the nonlinear hysteresis block can be approximated as

$$\begin{aligned} h(y+l, \dot{y}) &\simeq h(y_1 + l, \dot{y}_1) \\ &\simeq \mathrm{Re}\big[N_0 A + N_1 B\mathrm{e}^{i\omega t}\big] \end{aligned} \tag{14}$$

where

$$\begin{cases} N_0 = N_0(A, B, \omega) := \frac{1}{A}\frac{1}{T}\int_0^T h(y_1(t) + l, \dot{y}_1(t))\,\mathrm{d}t, \\ N_1 = N_1(A, B, \omega) := \frac{1}{B}\frac{2}{T}\int_0^T h(y_1(t), \dot{y}_1(t))\mathrm{e}^{-i\omega t}\,\mathrm{d}t \end{cases} \tag{15}$$

are the constant and harmonic gains of the nonlinear block also known as the describing functions of the nonlinearity [4]. We remark that $N_0 A$ and $N_1 B$ are the first two Fourier coefficients of $h(y_1(t) + l, \dot{y}_1(t))$, thus expression (15) represents a first order harmonic truncation. For the general class of hysteretic force models introduced, we obtain

$$\begin{aligned} N_0 &= \frac{1}{2\pi A}\sum_{n=1}^{N}\Bigg(\int_{-\pi}^{0} K_n^+ h_n(l + A + B\cos\tau)\,\mathrm{d}\tau \\ &\quad + \int_0^{+\pi} K_n^- h_n(l + A + B\cos\tau)\,\mathrm{d}\tau\Bigg) \\ &= \frac{1}{2\pi A}\sum_{n=1}^{N} K_n^{(s)}\int_0^{+\pi} h_n\big[B(q + \cos\tau)\big]\,\mathrm{d}\tau \end{aligned}$$

where

$$K_n^{(s)} := K_n^- + K_n^+ \tag{16}$$

and

$$q := \frac{l + A}{B}\,. \tag{17}$$

Similarly, we find for N_1

$$\begin{aligned} N_1 &= \frac{1}{\pi B}\sum_{n=1}^{N}\Bigg(\int_{-\pi}^{0} K_n^+ h_n\big[B(q + \cos\tau)\big]\mathrm{e}^{-i\tau}\,\mathrm{d}\tau \\ &\quad + \int_0^{+\pi} K_n^- h_n\big[B(q + \cos\tau)\big]\mathrm{e}^{-i\tau}\,\mathrm{d}\tau\Bigg) \\ &= \frac{1}{\pi B}\sum_{n=1}^{N}\Bigg(K_n^{(s)}\int_0^{+\pi} h_n\big[B(q + \cos\tau)\big]\cos\tau\,\mathrm{d}\tau \\ &\quad - i\,K_n^{(d)}\int_0^{+\pi} h_n\big[B(q + \cos\tau)\big]\sin\tau\,\mathrm{d}\tau\Bigg) \end{aligned} \tag{18}$$

where

$$K_n^{(d)} := K_n^+ - K_n^-\,. \tag{19}$$

Substituting in (5), assuming a sinusoidal forcing $\gamma(t) = \mathrm{Re}[\Gamma e^{i(\omega t+\phi)}]$, yields the relation

$$A + Be^{i\omega t} = -L(0)N_0 A + L(i\omega)\big[-N_1 B + \Gamma e^{i\phi}\big]e^{i\omega t} \quad \text{for all } t \tag{20}$$

or, equivalently the relations,

$$\begin{cases} [1 + L(0)N_0(A,B)]A = 0 \quad \text{and} \\ [1 + L(i\omega t)N_1(A,B)]B = L(i\omega t)\Gamma e^{i\phi}. \end{cases} \tag{21}$$

Finally, we can easily decouple the variable ϕ from (21) as follows

$$\begin{cases} [1 + L(0)N_0(A,B)]A = 0, \\ |1 + L(i\omega t)N_1(A,B)|B = |L(i\omega t)|\Gamma, \\ \phi = \arg[L(i\omega)^{-1} + N_1(A,B)]. \end{cases} \tag{22}$$

Equations (22) represent a system of three nonlinear equations in the three unknown A, B, ϕ. By solving it, we can find the sinusoidal approximation of $y(t)$ given by (13).

4.1 Piecewise interaction model analysis

For the piecewise-linear potential described in Sect. 3.1, we obtain

$$\begin{cases} N_0 = \frac{1}{A}[K_1^{(s)} R_1(q) + K_2^{(s)} R_2(q) B], \\ N_1 = \frac{1}{B}[K_1^{(s)} S_1(q) + iK_1^{(d)} T_1(q)] \\ \qquad + [K_2^{(s)} S_2(q) + iK_2^{(d)} T_2(q)] \end{cases} \tag{23}$$

where $R_1(q) := \frac{\mathrm{acos}(q)}{2\pi}$, $R_2(q) := \frac{q\,\mathrm{acos}(q) - \sqrt{1-q^2}}{2\pi}$, $S_1(q) := -\frac{\sqrt{1-q^2}}{\pi}$, $S_2(q) := \frac{\mathrm{acos}(q) - q\sqrt{1-q^2}}{2\pi}$, $T_1(q) := \frac{1-q}{\pi}$ and $T_2(q) := -\frac{(1-q)^2}{2\pi}$. Finally, by substitutions $\chi(q) := K_1^{(s)} R_1(q)$, $\Omega(q) := K_2^{(s)} R_2(q)$, $\Phi(q) := K_1^{(s)} S_1(q) + iK_1^{(d)} T_1(q)$ and $\Psi(q) := K_2^{(s)} S_2(q) + iK_2^{(d)} T_2(q)$ we can obtain for the describing functions

$$N_0 = \frac{1}{A}\big[\chi(q) + \Omega(q)B\big],$$

$$N_1 = \frac{\Phi(q)}{B} + \Psi(q).$$

In this model, the variable q represents the "penetration" of the tip into the sample. In fact, assuming as exact the first harmonic approximation, we have that for $q > 1$ the tip does not get in contact with the sample; for $q = 1$, the tip grazes the sample, and for $q < 1$, the tip enters the sample. The case $q < -1$ does not have a physical meaning in this model. From (21), it is also possible to write B as a function of q. In fact,

$$B = \frac{\Gamma}{|L(i\omega)^{-1} + N_1|} \tag{24}$$

implies

$$\big|L(i\omega)^{-1}B + BN_1\big|^2 = \big|L(i\omega)^{-1}B + \Phi + \Psi B\big|^2 = \Gamma^2. \tag{25}$$

The substitutions $\hat{\Phi} := \Phi$ and $\hat{\Psi} := \Psi + L(i\omega)^{-1}$ yield

$$(\hat{\Phi} + \hat{\Psi}B)\big(\hat{\Phi}^* + \hat{\Psi}^* B\big) = \Gamma^2 \tag{26}$$

which implies that

$$|\hat{\Psi}|^2 B^2 + 2\,\mathrm{Re}\big[\hat{\Phi}\hat{\Psi}^*\big]B + |\hat{\Phi}|^2 - \Gamma^2 = 0. \tag{27}$$

Equation (27) is a simple second order algebraic equation whose roots are

$$B(q) = \frac{-\mathrm{Re}[\hat{\Phi}\hat{\Psi}^*]}{|\hat{\Psi}|^2} \pm \frac{\sqrt{\mathrm{Re}[\hat{\Phi}\hat{\Psi}^*]^2 - |\hat{\Psi}|^2(|\hat{\Phi}|^2 - \Gamma^2)}}{|\hat{\Psi}|^2}. \tag{28}$$

Substituting in (22) and noting that $l = qB - A$, we can write

$$A(q) = -L(0)\big[\chi(q) + \Psi(q)B(q)\big], \tag{29}$$

$$\phi(q) = \arg\big[L(i\omega)^{-1} + N_1\big(A, B(q)\big)\big], \tag{30}$$

$$l(q) = qB(q) + L(0)\big[\chi(q) + \Psi(q)B(q)\big]. \tag{31}$$

The variable q (17), depends on A, B, and l (see (17)), therefore, (29–31) are implicit relations. Equations (29–31) make up a system which cannot be solved in closed form since it involves transcendental functions. However, it is possible to obtain its solution through a conceptually easy method. Assuming that l is a known parameter of the model, it is possible by (31) to determine the corresponding values of q and then A, B, and ϕ by exploiting (29) and (30). In other words, we have transformed the problem of solving the system given by (29), (30), and (31) into

the easier problem of solving a single real equation in the unknown q.

Experimentally, the amplitude-separation curve is obtained by slowly moving the sample toward the cantilever and measuring both the amplitude of the first harmonic and the separation. Although it is not possible to derive an explicit analytical form for $B = B(l)$, we can give a parametric form for it. By using the "q-explicit" (29–31), we can consider the parametric curve

$$\begin{cases} l = l(q) \\ B = B(q) \end{cases} \quad \text{for all } q \in \mathbf{R}. \tag{32}$$

4.2 Lennard–Jones like hysteretic model analysis

For the generic hysteretic interaction force of the class (12), we can evaluate the describing functions N_0 and N_1 of the nonlinearity h:

$$\begin{cases} N_0 = \sum_{n=1}^{N} \frac{K_n^{(s)}}{AB^n} R_n(q), \\ N_1 = \sum_{n=1}^{N} \frac{1}{B^{n+1}} [K_n^{(s)} S_n(q) + i K_n^{(d)} T_n(q)] \end{cases}$$

where the functions

$$R_n(q) := \frac{1}{2\pi} \int_0^{\pi} \frac{1}{(q + \cos\tau)^n} \mathrm{d}\tau,$$

$$S_n(q) := \frac{1}{\pi} \int_0^{\pi} \frac{\cos\tau}{(q + \cos\tau)^n} \mathrm{d}\tau,$$

$$T_n(q) := \frac{1}{\pi} \int_0^{\pi} \frac{-\sin\tau}{(q + \cos\tau)^n} \mathrm{d}\tau$$

can be analytically evaluated for any given n and $q > 1$. Imposing harmonic balance, we get

$$A = -L(0) \sum_{n=1}^{N} K_n^{(s)} \frac{R_n(q)}{B^n}, \tag{33}$$

$$\left[\Gamma \mathrm{e}^{i\phi} - \sum_{n=1}^{N} \frac{K_n^{(s)} S_n(q) + i K_n^{(d)} T_n(q)}{B^n} \right] L(i\omega) = B. \tag{34}$$

Equation (34) can be expressed in the form

$$L(i\omega)\Gamma \mathrm{e}^{i\phi} = L(i\omega) \sum_{n=1}^{N} \frac{K_n^{(s)} S_n(q) + i K_n^{(d)} T_n(q)}{B^n} + B. \tag{35}$$

We can remove ϕ from (35) by multiplying each term by its conjugate. Finally, multiplying by B^{2N} the equation can be rewritten as a $(N+2)$-degree polynomial in the variable B whose coefficients depend only on the variable q

$$p(B) = \sum_{n=1}^{2N+2} C_n(q) B^n = 0. \tag{36}$$

It can be shown that $C_{2N+2} = 1/|L(i\omega)|^2$, $C_{2N+1} = 0$ and $C_{2N} = -\Gamma^2$. For sufficiently large q (that is, when the interaction is negligible), we have that $C_k \cong 0$, for all $k < 2N$, therefore,

$$p(B) \cong \left(\left| L(i\omega) \right|^{-2} B^2 - \Gamma^2 \right) B^{2N} = 0. \tag{37}$$

One root of the equation above is $B \cong \Gamma |L(i\omega)|$. This solution corresponds to the free oscillation amplitude that the cantilever assumes when the sample is far away and does not influence the cantilever dynamics. For every $q > 1$, the polynomial equation (36) can be solved in B. Only the solutions that are real and positive have relevance. The constant component of the periodic solution A can be evaluated exploiting (33). The phase ϕ can also be similarly obtained as a function of the parameter q and is given by

$$\phi(q) = \arg \left\{ L^{-1}(i\omega) + \sum_{n=1}^{N} \frac{K_n^{(s)} S_n(q) + i K_n^{(d)} T_n(q)}{B^{n+1}} \right\}. \tag{38}$$

Finally, the parameter l is given by the original relation

$$l(q) = q B(q) - A(q). \tag{39}$$

The final result is that the variables A, B, ϕ, and l are all expressed with respect to the parameter q. The amplitude-separation diagram can be obtained considering the pair $(l(q), B(q))$ which describes a curve in a parametric form. A similar procedure can be used to obtain the relation between any two variables with no need of simulation tools.

In [18] and [16], it is shown that the approximation error of the HB method for the analysis of this model is negligible when compared to results obtained by simulating the same model.

5 Identification of the tip-sample force model

In this section, we present methods to identify parameters of the hysteresis based models developed earlier. As previously discussed, the frequency response $L(i\omega)$ is known since it can be independently estimated. We also assume that the separation l can be changed by means of the piezo actuator placed beneath the sample. Therefore, we can consider a set of M experiments with different values of l

$$l_m := l_0 + md, \quad m = 1, \dots, M \tag{40}$$

where l_0 is a fixed offset and $d > 0$ is a suitable separation step. For every l_m, the quantities A_m, B_m, ϕ_m can be evaluated from the measured signal $y(t)$ after it has reached its steady state, and q_m can be computed from (17).

The functions (8) chosen to model the interaction have the useful property that they are linear in the parameters K_n^- and K_n^+, or as is evident from (16) and (19) in $K_n^{(s)}$ and $K_n^{(d)}$. The linear dependence on the parameters aids their identification using the harmonic balance relations (22). The first order harmonic balance equations lead to a set of M linear equations in the $2N$ unknown variables $K_n^{(s)}$ and $K_n^{(d)}$

$$\begin{cases} \Gamma\cos(\phi_m) - \mathrm{Im}[L^{-1}(i\omega)]B_m = \sum_{n=1}^{N} K_n^{(s)} \frac{S_n(q_m)}{B^{n+1}}, \\ \Gamma\sin(\phi_m) - \mathrm{Re}[L^{-1}(i\omega)]B_m = \sum_{n=1}^{N} K_n^{(d)} \frac{T_n(q_m)}{B^{n+1}}, \\ m = 1, \dots, M. \end{cases} \tag{41}$$

Assuming that there are $M > 2N$ experimental data point and adopting a more compact notation, we can write two independent matrix equations

$$\begin{aligned} P_S K^{(s)} &= Q_S, \\ P_D K^{(d)} &= Q_D \end{aligned} \tag{42}$$

where

$$K^{(s)} := \begin{pmatrix} K_1^{(s)} \\ \vdots \\ K_n^{(s)} \end{pmatrix} \quad \text{and} \quad K^{(d)} := \begin{pmatrix} K_1^{(d)} \\ \vdots \\ K_n^{(d)} \end{pmatrix} \tag{43}$$

are the unknown vectors and

$$\begin{aligned} P_S[m,n] &:= \frac{S_n(q_m)}{B_m^{n+1}}, \\ Q_S[m] &:= \Gamma\cos(\phi_m) - \mathrm{Re}\big[L^{-1}(i\omega)\big]B_m, \end{aligned}$$

$$\begin{aligned} P_D[m,n] &:= \frac{T_n(q_m)}{B_m^{n+1}}, \\ Q_D[m] &:= \Gamma\sin(\phi_m) - \mathrm{Im}\big[L^{-1}(i\omega)\big]B_m \end{aligned} \tag{44}$$

are constant matrices.

Since the number of equations is greater than the number of unknowns, (42) is not expected to be feasible. A common strategy is to find the set of parameters which better fits the equations according to the quadratic cost function

$$\begin{aligned} &V\big(l_0, K^{(s)}, K^{(d)}\big) \\ &\quad = \big\| Q_S - P_S K^{(s)} \big\|^2 + \big\| Q_D - P_D K^{(d)} \big\|^2, \end{aligned} \tag{45}$$

where we have stressed the dependence on the offset l_0 since it is not a priori known. Thus, the optimal values $\tilde{K}^{(s)}$ and $\tilde{K}^{(d)}$ can be evaluated casting an optimization problem which also takes into account the constraints (9)

$$\big(\tilde{K}^{(s)}(l_0), \tilde{K}^{(d)}(l_0)\big) = \arg \min_{\substack{K^{(s)} \\ K^{(d)} \le 0}} V\big(l_0, K^{(s)}, K^{(d)}\big). \tag{46}$$

We remark that forcing the condition $K^{(d)} = 0$ in (46) is equivalent to the assumption of a interaction force with no hysteresis, and, therefore, conservative.

Given l_0, problem (46) is a quadratic optimization problem with linear constraints. Many algorithms are known in literature to determine its solution $(\tilde{K}^{(s)}(l_0), \tilde{K}^{(d)}(l_0))$ [19]. Finally, we can estimate the offset l_0 by the solution of the following problem

$$\tilde{l}_0 = \arg\min_{l_0} V\big(l_0, \tilde{K}^{(s)}(l_0), \tilde{K}^{(d)}(l_0)\big), \tag{47}$$

which is another minimization over a scalar variable, solvable griding the parameter space. The identified parameters are $(\tilde{K}^{(s)}(\tilde{l}_0), \tilde{K}^{(d)}(\tilde{l}_0))$.

6 Experimental results

An atomic force microscope (Multimode from Digital Instruments, Santa Barbara, CA) was operated in dynamic mode using a silicon cantilever of 225 μm in length. Using a thermal-response based approach the cantilever was identified with a second order linear oscillator with natural frequency $\omega_n = 2\pi 73.881$ rad/s

and damping factor $\xi = 0.00378$. The nominal spring constant k and the nominal frequency resonance of the cantilever were 4 N/m and 70 KHz, respectively. A sinusoidal voltage with frequency ω_n was applied to the dither piezo in order to make the cantilever oscillate. Experiments were performed on a silicon wafer sample. The separation amplitude curve has been experimentally measured during the approach and retract phases. The approach and the retract force curves show a jump phenomenon occurring at two different values of the separation (dashed and dotted curves in Fig. 5). Such phenomena are present and documented in literature [5]. The identification technique described in the previous section was employed using the data obtained during the retract phase only, while the data acquired during the approaching phase were used for validation purposes. The results obtained using the piecewise linear interaction model are reported in Fig. 5 (solid curve). The retract curve is well explained by the model data; this is not surprising as the data used to obtain the model parameters is the retract phase data. For the approach curve, a jump phenomenon occurring at a different separation is qualitatively well predicted, but it can be argued that it is not quantitatively satisfactory.

As a second case, the following simplified version of model (8) is used

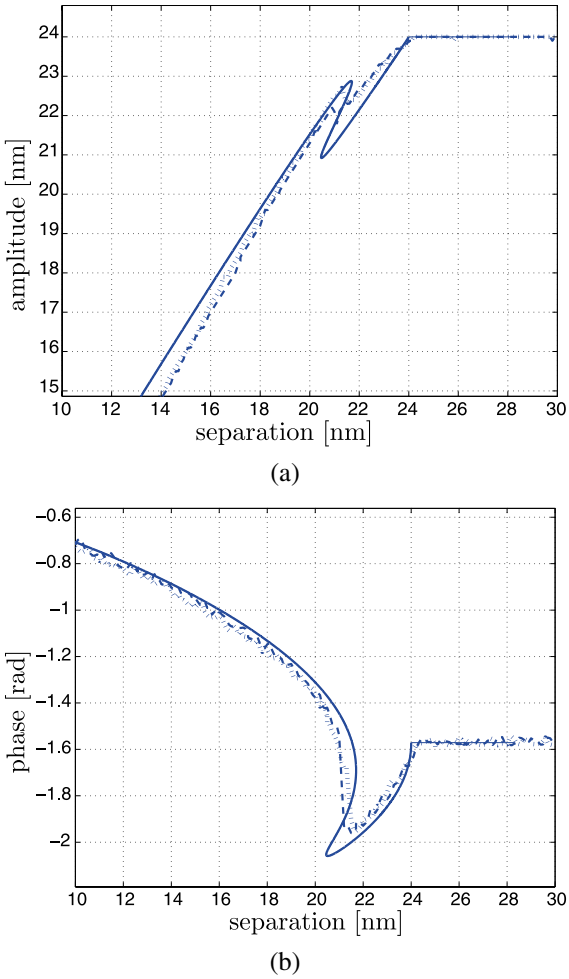

Fig. 5 Experimental amplitude (**a**) and phase (**b**) curves fitted using the piecewise linear model for the interaction force. *Solid line* is the curve obtained by the model; the *dashed* and the *dotted* ones are the experimental approach and retract curves, respectively

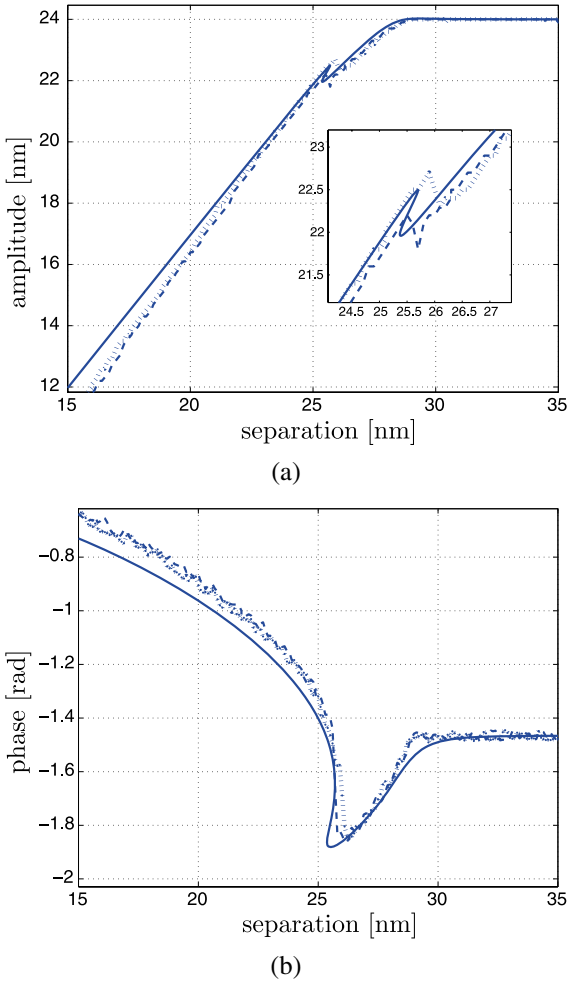

Fig. 6 Experimental amplitude (**a**) and phase (**b**) curves fitted using the Lennard–Jones model for the interaction force. *Solid line* is the curve obtained by the model; the *dashed* and the *dotted* ones are the experimental approach and retract curves, respectively

$$h(\delta,\dot{\delta}) = \begin{cases} \frac{K_7^-}{\delta^7} + \frac{K_{13}^-}{\delta^{13}} & \text{if } \dot{\delta} < 0, \\ \frac{K_7^+}{\delta^7} + \frac{K_{13}^+}{\delta^{13}} & \text{if } \dot{\delta} > 0 \end{cases} \tag{48}$$

that is a standard Lennard–Jones potential function with a hysteresis dissipation. Identification results are shown in Fig. 6. As it is evident from the figure, the model predicts the discontinuity in the approach phase of the force curve accurately. The phase of the first harmonic is also predicted well by the model. As remarked in Figs. 5 and 6, harmonic balance has also allowed to reveal the presence of unstable periodic orbits (in the region in between the two jump points) and to clearly explain bifurcation phenomena in the system.

7 Conclusions

In the paper, we have proposed a class of models for tip-sample interaction in atomic force microscopy via impact dynamics. The use of a hysteresis model can be well combined with harmonic balance techniques for the analysis of oscillatory behavior to provide interesting insights into the dynamics. For instance, the presence of jump phenomena discovered in many experiments is well predicted and explained. The suggested method is based on a first order harmonic approximation and gives good quantitative results since the linear part of the considered Lur'e system shows a sharp filtering effect near the resonance frequency. In such a situation, the harmonic balance technique has advantages over standard numerical approaches since it requires a computational effort much smaller than the one required by simulation tools.

Acknowledgements This work was partially supported by the NSF grant CMS-0626171.

References

1. Brogliato, B.: Nonsmooth Mechanics: Models Dynamics and Control. Springer, New York (1999)
2. Brach, R.: Mechanical Impact Dynamics: Rigid Body Collisions. Wiley, New York (1991)
3. Fontaine, P., Guenon, P., Daillant, J.: A critical look at surface force measurement using a commercial atomic force microscope in the noncontact mode. Rev. Sci. Instrum. **68**, 4145–4151 (1997)
4. Khalil, H.K.: Nonlinear Systems. Prentice-Hall, Upper Saddle River (1996)
5. Kühle, A., Sorensen, A.H., Bohr, J.: Role of attractive forces in tapping tip force microscopy. J. Appl. Phys. **81**, 6562–6569 (1997)
6. Sebastian, A., Salapaka, M., Chen, D.: Harmonic and power balance tools for tapping-mode afm. J. Appl. Phys. **89**, 6473–6480 (2001)
7. Holscher, H.: Quantitative measurement of tip-sample interactions in amplitude modulation atomic force microscopy. Appl. Phys. Lett. **89**, 123109 (2006)
8. Salapaka, M., Chen, D., Cleveland, J.: Linearity of amplitude and phase in tapping-mode atomic force microscopy. Phys. Rev. B **61**, 1106–1115 (2000)
9. San Paulo, A., García, R.: Tip-surface forces, amplitude, and energy dissipation in amplitude-modulation (tapping mode) force microscopy. Phys. Rev. B **64**, 193411 (2001)
10. Cappella, B., Dietler, G.: Force distance by atomic force microscopy. Surf. Sci. Rep. **34**, 1–104 (1999)
11. Basso, M., Genesio, R., Tesi, A., Torrini, G.: On describing systems with periodic behaviour in terms of simple nonlinear models. In: Proceedings of Conference Control of Oscillations and Chaos, Saint-Petersburg, Russia, August (1997)
12. Basso, M., Genesio, R., Tesi, A.: A frequency method for predicting limit cycle bifurcations. Nonlinear Dyn. **13**, 339–360 (1997)
13. Gibson, C., Smith, D., Roberts, C.: Calibration of silicon atomic force microscope cantilevers. Nanotechnology **16**, 234–238 (2005)
14. Lee, M., Jhe, W.: General theory of amplitude-modulation atomic force microscopy. Phys. Rev. Lett. **97**, 036104 (2006)
15. Garcia, R., Gomez, C.J., Martinez, N.F., Patil, S., Dietz, C., Magerle, R.: Identification of nanoscale dissipation processes by dynamic atomic force microscopy. Phys. Rev. Lett. **97**(1–4), 016103 (2006)
16. Materassi, D., Basso, M., Genesio, R.: Frequency analysis of atomic force microscopes with repulsive-attractive interaction potentials. In: Proceedings of IEEE Conference on Decision and Control, Paradise Island, Bahamas, December (2004)
17. Israelachvili, J.N.: Intermolecular and Surface Forces. Academic Press, New York (1985)
18. Basso, M., Materassi, D.: Frequency analysis and identification in atomic force microscopy. Technical report, Dipartimento di Sistemi e Informatica (2006)
19. Boyd, S., Vandenberghe, L.: Convex Optimization. Cambridge University Press, Cambridge (2004)